

ARMY RESEARCH LABORATORY



Measured Degree of Infrared Polarization for a Variety of Thermal Emitting Surfaces

by Kristan P. Gurton, Rachid Dahmani, and Gordon Videen

ARL-TR-3240

June 2004

NOTICES

Disclaimers

The findings in this report are not to be construed as an official Department of the Army position unless so designated by other authorized documents.

Citation of manufacturer's or trade names does not constitute an official endorsement or approval of the use thereof.

Destroy this report when it is no longer needed. Do not return it to the originator.

Army Research Laboratory

Adelphi, MD 20783-1197

ARL-TR-3240

June 2004

Measured Degree of Infrared Polarization for a Variety of Thermal Emitting Surfaces

Kristan P. Gurton, Rachid Dahmani, and Gordon Videen
Computational and Information Sciences Directorate, ARL

REPORT DOCUMENTATION PAGE			Form Approved OMB No. 0704-0188	
<p>Public reporting burden for this collection of information is estimated to average 1 hour per response, including the time for reviewing instructions, searching existing data sources, gathering and maintaining the data needed, and completing and reviewing the collection information. Send comments regarding this burden estimate or any other aspect of this collection of information, including suggestions for reducing the burden, to Department of Defense, Washington Headquarters Services, Directorate for Information Operations and Reports (0704-0188), 1215 Jefferson Davis Highway, Suite 1204, Arlington, VA 22202-4302. Respondents should be aware that notwithstanding any other provision of law, no person shall be subject to any penalty for failing to comply with a collection of information if it does not display a currently valid OMB control number.</p> <p>PLEASE DO NOT RETURN YOUR FORM TO THE ABOVE ADDRESS.</p>				
1. REPORT DATE (DD-MM-YYYY) June 2004	2. REPORT TYPE Final	3. DATES COVERED (From - To) 9/2003 to 4/2004		
4. TITLE AND SUBTITLE Measured Degree of Infrared Polarization for a Variety of Thermal Emitting Surfaces			5a. CONTRACT NUMBER	
			5b. GRANT NUMBER	
			5c. PROGRAM ELEMENT NUMBER	
6. AUTHOR(S) Kristan P. Gurton, Rachid Dahmani, and Gordon Videen			5d. PROJECT NUMBER	
			5e. TASK NUMBER	
			5f. WORK UNIT NUMBER	
7. PERFORMING ORGANIZATION NAME(S) AND ADDRESS(ES) U.S. Army Research Laboratory ATTN: AMSRD-ARL-CI-EE 2800 Powder Mill Road Adelphi, MD 20783-1197			8. PERFORMING ORGANIZATION REPORT NUMBER ARL-TR-3240	
9. SPONSORING/MONITORING AGENCY NAME(S) AND ADDRESS(ES) U.S. Army Research Laboratory 2800 Powder Mill Road Adelphi, MD 20783-1197			10. SPONSOR/MONITOR'S ACRONYM(S)	
			11. SPONSOR/MONITOR'S REPORT NUMBER(S)	
12. DISTRIBUTION/AVAILABILITY STATEMENT Approved for public release; distribution unlimited.				
13. SUPPLEMENTARY NOTES				
<p>14. ABSTRACT</p> <p>We report on a series of parametric measurements designed to measure the attenuative effects that surface roughness and aerosol contamination play in reducing polarized thermal surface emission. In particular, we measure the spectrally resolved linear degree of polarization (LDOP) for a series of roughened borosilicate (Pyrex¹) glass substrates as a function of roughness parameter, Ra, root mean square slope, m, and the angle of observation, θ. Spectrally resolved LDOP is measured over the waveband region 4 to 13 μm by a modified Fourier transform IR spectrometer in which a wire-grid polarizer and an achromatic quarter-wave plate are used in conjunction to measure all four Stokes parameters.</p> <p>A second set of measurements is conducted on similar smooth glass substrates that are subjected to varying degrees of dew formation and aerosol contamination. Test substrates are oriented at a high grazing angle of 80 degrees and placed in a closed chamber. Dew or attenuative particulates, i.e., carbon black, potassium bromide, or pollen particles, are allowed to condense/settle on the thermal emitting surface while a band-averaged LDOP is recorded with a long-wave polarimetric IR imaging system. Measured results are then compared with predictive calculations based on a weighted Fresnel relation.</p>				
<p>¹Pyrex® is a registered trademark of Corning.</p>				
15. SUBJECT TERMS Polarization, infrared, dew, surface contamination				
16. SECURITY CLASSIFICATION OF: a. REPORT Unclassified		17. LIMITATION OF ABSTRACT UL	18. NUMBER OF PAGES 33	19a. NAME OF RESPONSIBLE PERSON Kristan Gurton
b. ABSTRACT Unclassified		19b. TELEPHONE NUMBER (Include area code) 301-394-2093		

Contents

List of Figures	iv
Acknowledgments	vi
1. Introduction	1
2. Experiment: Surface Roughness	4
3. Results: Surface Roughness	7
4. Experiment: Dew Formation and Aerosol Contamination	11
5. Results: Dew Formation and Aerosol Contamination	17
6. Discussion	19
7. References	23
Distribution List	25

List of Figures

Figure 1. Complex indices of refraction used for the borosilicate (Pyrex) glass plates (14).....	4
Figure 2. Measured rms slope distribution for the three roughened borosilicate (Pyrex) glass substrates. (Here we have assumed a Gaussian distribution.)	5
Figure 3. Simple schematic showing the experimental setup used during the surface roughness spectro-polarimetric measurement.....	5
Figure 4. Measured LDOP as a function of wavelength and angle of incidence for a <i>smooth</i> borosilicate glass substrate heated to 65 °C. (Also shown [triangular data points] is the corresponding calculated LDOP for an emission wavelength of 9.28 μm based on the Fresnel relations of equations 4 through 6.).....	8
Figure 5. Measured LDOP for a lightly roughened borosilicate plate with Ra=3.98μm and rms slope=9.67 degrees, as a function of wavelength and angle of incidence. (Plate temperature was held at 65 °C.)	8
Figure 6. Measured LDOP for a moderately roughened borosilicate plate with Ra=4.80μm and rms slope=8.60 degrees, as a function of wavelength and angle of incidence. (Plate temperature was held at 65 °C.)	9
Figure 7. Measured LDOP for a very rough borosilicate plate with Ra=6.68μm and rms slope=11.90 degrees, as a function of wavelength and angle of incidence. (Plate temperature was held at 65 °C.)	9
Figure 8. Measured LDOP as a function of wavelength and angle of incidence for a smooth borosilicate plate coated with a thin layer of black Krylon paint. (Plate temperature was held at 65 °C.)	10
Figure 9. Measured LDOP as a function of wavelength and angle of incidence for a smooth borosilicate plate coated with a thin layer of a green CARC paint. (Plate temperature was held at 65 °C.)	11
Figure 10. Diagram showing the experimental setup used for the dew/aerosol contamination study. (The test plate is oriented at a fixed angle of 80 degrees and held at room temperature.)	12
Figure 11. Video image series showing the dew condensation process. (Shown in each image is the corresponding coverage ratio, [i.e., surface area covered divided by the total area], and the corresponding measured LDOP for $\theta=80^\circ$.)	14
Figure 12. Sample calibrated LWIR polarimetric image used to determine the LDOP for a smooth glass substrate contaminated by a modest amount of carbon black particles. (LDOP is determined from the gray scale values for the pixels that represent the heated glass surface.).....	15
Figure 13. Sample visible images showing various forms of aerosols contamination considered, i.e., orchard pollen (top left), carbon black (top right), and KBr particles (bottom).....	16

Figure 14. Measured LDOP for varying degrees of dew (water) coverage on the surface of a smooth borosilicate glass substrate at 22 °C, $\theta=80^\circ$. (Also shown is the calculated LDOP by the geometric approach of Videen (12).)	18
Figure 15. Measured LDOP for a smooth borosilicate glass plate held at 22 °C, contaminated with varying degrees of carbon black, KBr particles, or pollen, that were evenly dispersed on the surface. (Substrates mounted at $\theta=80^\circ$ [the dashed line shown represents the corresponding curve fit]. Also shown is the calculated LDOP based on the geometric approach put forth by Videen.)	18
Figure 16. Comparison of measured LDOP (taken at 9.90 μm) as a function substrate orientation for various roughened glass plates. (Also shown are the measured and Fresnel-based calculations for smooth glass substrates [top dashed line] and results from Jordan and Lewis [bottom dashed line] (7).)	20

Acknowledgments

We would like thank Dr. Huey Anderson of the U.S. Army Aviation and Missile Command for his continued support and assistance in conducting this research. Also we would like to thank Dr. David Chenault, Mr. Graig Farlow, and Mr. Michael Gulley of SY Technologies, Inc., for their insight and development of the LWIR polarimetric camera system used in research.

1. Introduction

It is generally accepted that smooth surfaces emit thermal radiation that is partially polarized, depending on the angle of observation (1,2). This induced polarized emission originates from differences in orthogonal components of the directional spectral emissivity, $\varepsilon(\lambda, T, \theta, \phi)$ (3).

Because many man-made objects tend to possess surface structures that are more uniform when compared to common, naturally occurring background materials (e.g., soil, vegetation, trees, etc.), it has been suggested that by examining the polarization state of the IR image forming radiation, one can significantly improve the ability to see objects that are obscured by background clutter (4,5,6).

In order to understand the conditions necessary for polarized thermal emission to occur, we start by considering an object with a planar surface bound by air with directional spectral emissivity, $\varepsilon(\lambda, T, \theta, \phi)$. By considering the steady state form of Kirchhoff's law, we can express directional spectral emissivity in terms of the directional spectral absorptivity, $\alpha(\lambda, T, \theta, \phi)$, and reflectivity, $r(\lambda, T, \theta, \phi)$, i.e.,

$$\varepsilon(\lambda, T, \theta, \phi) = \alpha(\lambda, T, \theta, \phi) = 1 - r(\lambda, T, \theta, \phi). \quad (1)$$

The angles ϕ and θ represent the surface azimuth and the angle between the surface normal, \hat{n} , and the detector's line of sight (LOS), respectively.

If we now express the total emissivity in terms of two orthogonal components, ε_{\perp} and ε_{\parallel} , we have

$$\varepsilon(\lambda, T, \theta, \phi) = \frac{\varepsilon_{\perp}(\lambda, T, \theta, \phi) + \varepsilon_{\parallel}(\lambda, T, \theta, \phi)}{2} \quad (2)$$

in which the symbols \perp and \parallel designate the directions perpendicular and parallel to the plane of emission, i.e., the plane defined by the surface normal and the LOS. Similarly, by expressing the absorptivity and reflectivity in terms of their orthogonal components, we find that ε_{\perp} and ε_{\parallel} can be expressed as

$$\varepsilon_{\perp}(\lambda, T, \theta, \phi) = \alpha_{\perp}(\lambda, T, \theta, \phi) = 1 - r_{\perp}(\lambda, T, \theta, \phi) \quad (3a)$$

$$\varepsilon_{\parallel}(\lambda, T, \theta, \phi) = \alpha_{\parallel}(\lambda, T, \theta, \phi) = 1 - r_{\parallel}(\lambda, T, \theta, \phi). \quad (3b)$$

Let us now define a linear degree of emission polarization, $LDOP(\lambda, \theta)$, as the difference between the two orthogonal emissivities divided by the total emittance. We find

$$LDOP(\lambda, \theta) = (\varepsilon_{\perp}(\lambda, \theta) - \varepsilon_{\parallel}(\lambda, \theta)) / (\varepsilon_{\perp}(\lambda, \theta) + \varepsilon_{\parallel}(\lambda, \theta)), \quad (4)$$

in which we have temporarily omitted the temperature dependences for brevity. By representing the reflectivity in terms of Fresnel coefficients, we find two representations for the orthogonal components of the emissivity, depending on whether the emitting surface is a dielectric or a metal (3).

For a moderately absorbing dielectric surface, we find

$$\varepsilon_{\perp}(\lambda, \theta) = 1 - \left\{ \frac{((n(\lambda) - ik(\lambda))^2 - \sin^2 \theta)^{1/2} - \cos \theta}{((n(\lambda) - ik(\lambda))^2 - \sin^2 \theta)^{1/2} + \cos \theta} \right\}^2 \quad (5a)$$

$$\varepsilon_{\parallel}(\lambda, \theta) = 1 - \left\{ \frac{(n(\lambda) - ik(\lambda))^2 - \cos \theta - ((n(\lambda) - ik(\lambda))^2 - \sin^2 \theta)^{1/2}}{(n(\lambda) - ik(\lambda))^2 - \cos \theta + ((n(\lambda) - ik(\lambda))^2 - \sin^2 \theta)^{1/2}} \right\}^2 \quad (5b)$$

and for a pure metallic surface,

$$\varepsilon_{\perp}(\lambda, \theta) = \frac{4n(\lambda) \cos \theta}{\cos^2 \theta + 2n(\lambda) \cos \theta + n^2(\lambda) + k^2(\lambda)} \quad (6a)$$

$$\varepsilon_{\parallel}(\lambda, \theta) = \frac{4n(\lambda) \cos \theta}{(n^2(\lambda) + k^2(\lambda)) \cos^2 \theta + 2n(\lambda) \cos \theta + 1} \quad (6b)$$

in which air is assumed to be surrounding the surface with the index of refraction taken to be 1, and the complex refractive index for the surface is defined as $m(\lambda) = n(\lambda) - ik(\lambda)$.

Equations 4 through 6 are valid only for smooth, homogenous surfaces that are contamination free. As a result, the predicted linear degree of polarization (LDOP) expressed by equation 4 should be considered an ideal case. Minor surface anomalies can result in great differences between measured and calculated LDOP.

Various models have been proposed to calculate the attenuation seen in the polarized emission when the surface in question is either roughened or contaminated by small particles. Jordan and Lewis first reported both measured and calculated attenuated thermal emission over the waveband 10 to 11 μm for a series of roughened glass and aluminum substrates as a function of surface orientation and a measured slope distribution (7,8). In their report, they present a modified Fresnel model that effectively weights the predicted emissivity by the normalized slope distribution. They report good agreement between measured and calculated LDOP for light to moderately roughened surfaces, but agreement was less certain as the roughened facets became larger.

Separately, both Shaw and Chang expand on the slope-weighted Fresnel approach by taking into account facet shadowing and multiple scattering (9,10,11). Similar to the Jordan approach, they treat the roughened surface as a series of infinitesimally small planar facets and integrate over all possible orientations described by the normalized slope distribution.

Recently, Videen has proposed a geometric model that describes the attenuation of polarized emittance for smooth surfaces that become contaminated by a varying density of small spherical particles (12).

Regardless of the type of surface anomaly, most models attribute the attenuation of polarized emission to a reduction of the effective emitting area; i.e., surfaces that are rough or partially covered by contaminating particles reduce the effective area that contributes to the polarized emission.

In order to understand how polarized thermal emission is affected by various surface conditions, a series of spectral IR polarimetric measurements is conducted on a variety of modified substrates.

In particular, the LDOP is measured at various angles of observation for a variety of well-characterized glass substrates that were either a) roughened to varying degrees by sand blasting of the plates, or b) exposed to varying degrees of aerosol or dew formation.

For studies concerning substrates that are roughened, the LDOP is measured over the entire wavelength region of 4 to 13 μm . A polarimetrically modified Fourier transform IR interferometer (FTIR) is used to measure the spectrally resolved Stokes parameters, S0, S1, S2, S3, and thus, the resultant LDOP, for different surface orientations angles and measured roughness slope distributions (13).

For surfaces contaminated by aerosol/dew formation, a prototype long wavelength infrared (LWIR) imaging polarimeter was used to measure the LDOP. The polarimetric imaging system effectively measures the band-averaged LDOP over the wavelength region, 8.5 to 10.5 μm . The LWIR polarimetric camera is developed by SY Technologies, Inc., Huntsville, AL, and uses a proprietary optic design in which a spinning wave-plate retarder is placed at the focal plane of the focal plane array (FPA). As a result, SY Technologies, Inc., reports pixel mis-registration of less than 1/10 of a pixel. The imaging system is designed to produce well-calibrated real-time polarimetric and/or stokes video imagery.

Three types of particulates are considered for the aerosol contamination portion of the study. Contamination by absorbing, transparent, and semi-transparent aerosol particles is examined, i.e., carbon black, potassium bromide (KBr) particles, and orchard grass pollen, respectively. Finally, all measured LDOP values are compared with a predicted LDOP value based on a simple geometric model that uses an effective “coverage ratio” as a primary input, i.e., we define the coverage ratio as the area covered by the contaminant divided by the total area, when viewed along the surface normal.

2. Experiment: Surface Roughness

Borosilicate glass (Pyrex¹) plates are chosen as the sample substrate because of their initial smoothness, readily available indices of refraction, and a high emissivity value of 0.94. Figure 1 shows the complex indices of refraction used in our Fresnel calculations for the plates (14). Three-inch square glass plates are sand blasted with various types of abrasives and pressures. Surface roughness (R_a) and the root mean square (rms) slope, m_0 , are measured for each plate at a number of different locations with a Teliform surface profilometer via American National Standards Institute standards. Because of the crystalline structure of the glass, a large variance in R_a values between samples was difficult to achieve. As a result, only four glass plates were considered, one smooth and three roughened. Values for the surface roughness R_a , were found to be 0.007 μm (smooth), 3.98 μm , 4.80 μm , and 6.68 μm (very rough), with the corresponding measured rms slope for the three roughened samples found to be 9.76, 8.60, and 11.90 degrees, respectively. Figure 2 shows the respective rms slope distributions where we have assumed a Gaussian form.

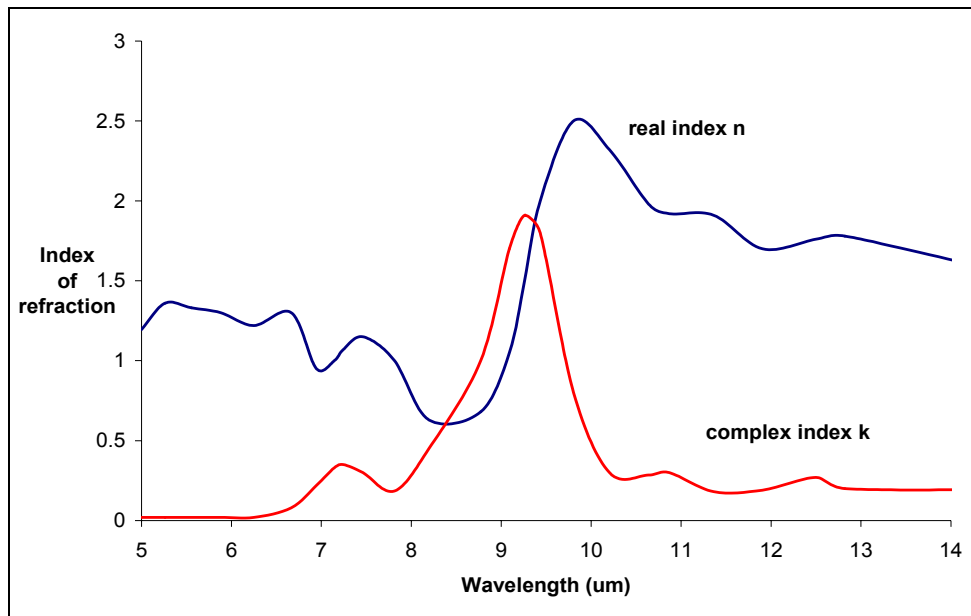


Figure 1. Complex indices of refraction used for the borosilicate (Pyrex) glass plates (14).

¹Pyrex® is a registered trademark of Corning.

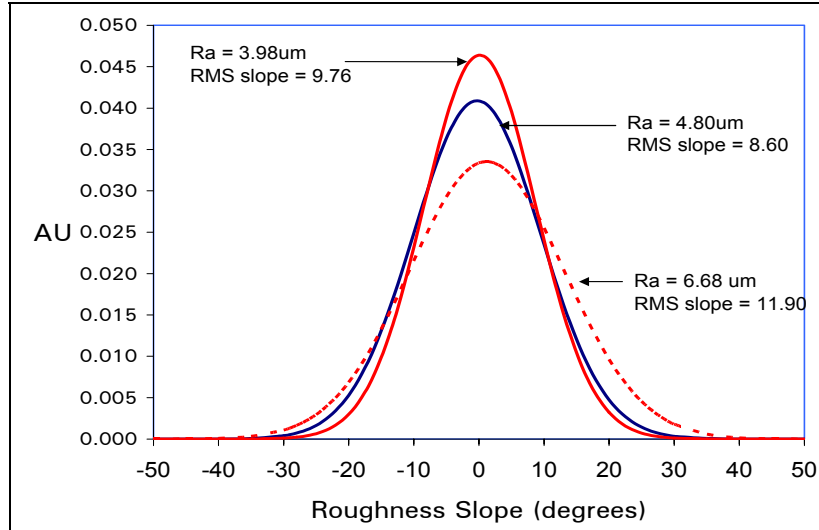


Figure 2. Measured rms slope distribution for the three roughened borosilicate (Pyrex) glass substrates. (Here we have assumed a Gaussian distribution.)

Borosilicate glass substrates are mounted to a brass heating element that is designed with a rotation $0^\circ \leq \theta \leq 90^\circ$, in which θ is the angle between the surface normal and the LOS. Thermal continuity between the substrate and the brass heating element is maintained by application of a thin layer of a heat-sink compound.

As mentioned earlier, the spectro-polarimetric measurements for roughened substrates are measured with a modified FTIR spectrometer. A simple diagram showing the various components of the experiment is seen in figure 3. An approximate 1-cm² region of the heated substrate is subtended by a f#10, barium fluoride (BaF_2) lens shown in the figure. The resultant collimated radiation is polarimetrically filtered with a IR wire-grid polarizer (extinction ratio of

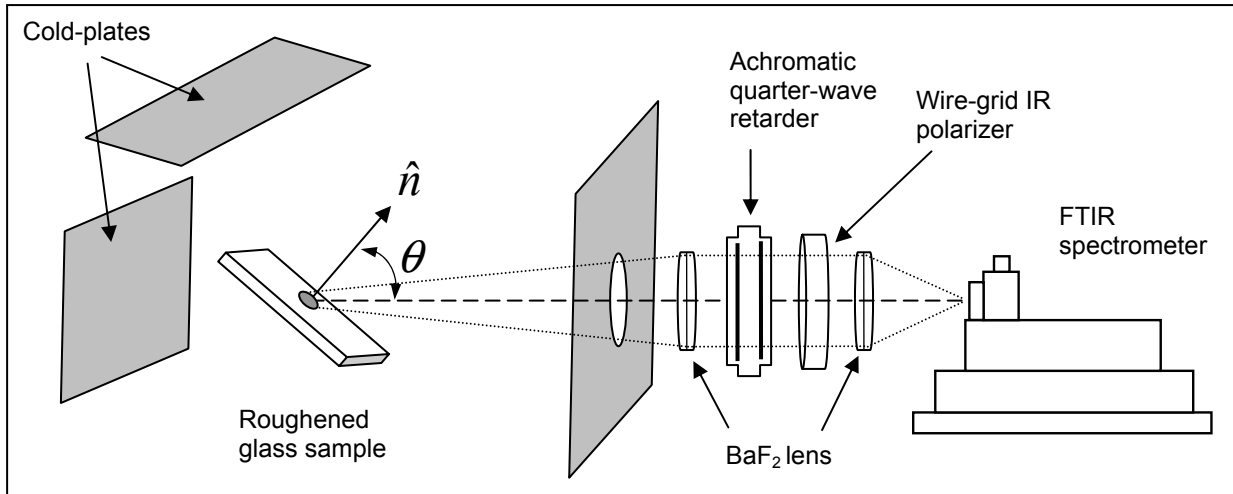


Figure 3. Simple schematic showing the experimental setup used during the surface roughness spectro-polarimetric measurement.

approximately 170) in conjunction with an achromatic zinc selenide (ZnSe) Fresnel rhomb quarter-wave plate. Filtered radiation is coupled to a Bomem FTIR spectrometer via a f#7 BaF₂ lens which effectively matched the entrance pupil of the spectrometer. This polarimetric configuration allows for analysis of select linear and circular polarized components necessary to calculate all four Stokes vectors, as well as the LDOP.

We keep polarization anomalies induced by the optics/instrumentation to a minimum by ensuring that all angles between the refracted rays and a particular optical element are kept to less than 20 degrees. This condition is easily achieved for polarimetric sampling optics but was less certain for the internal beam path of the FTIR. Crandall and Chipman analyzed the cross-beam configuration found in most conventional FTIRs and concluded that the aberrations induced by one arm of the interferometer/beam splitter perfectly cancel when combined with the second arm (15). Nevertheless, we did encounter a slight asymmetry in polarimetric response of the FTIR when randomly polarized thermal radiance is sampled. We attribute this relatively small polarimetric aberration to the dispersion inherent in the BaF₂ wire-grid polarizer. As a result, a minor correction is applied to all spectro-polarimetric data measured in order to compensate for the wavelength dependence of the polarizer.

Great effort is made to shield the measurement from ambient thermal radiation inherent to the laboratory. We achieved this by placing numerous “cold shields” at various locations around the experiment (see figure 3).

Target plates are heated to approximately 65 °C and are monitored with an embedded thermocouple. This temperature is sufficient to produce a good signal-to-noise (S/N) ratio when compared to the ambient levels generated within the laboratory. Each sample plate is oriented at a particular angle within the $0^\circ \leq \theta \leq 80^\circ$ range, at 10° increments, in which 0° orientation represents the condition when the surface normal is parallel to the LOS. A roughened sample plate is set at a given angle while the Fresnel rhomb and wire-grid polarizer are oriented in such a way to only pass linear states at 0°, 90°, ±45°, as well as the right- and left-handed circular states. Once a set of polarimetric data is measured, the angle of sample orientation is changed and the measurement is repeated.

Because no fine structure is expected in the polarimetric spectra, the FTIR was operated at a relatively modest resolution of 8 cm⁻¹, while a Bartlett apodization function is applied to each interferogram. The resultant interferogram is converted to an emission spectrum by the application of a Fourier transform.

The Stokes vectors that totally describe the polarization state of the thermal emission are calculated via the following relationships:

$$S0 = (S1^2 + S2^2 + S3^2)^{1/2} \quad (7)$$

in which S1, S2, and S3 are defined as

$$S1 = I(0) - I(90) \quad (8)$$

$$S2 = I(+45) - I(-45) \quad (9)$$

$$S3 = I(R) - I(L) \quad (10)$$

and $I(0)$, $I(90)$, $I(\pm 45)$ represent the recorded emission spectra for polarization states at 0, 90, ± 45 degrees, respectively, and $I(R)$ or $I(L)$ are measured spectra when only right- or left-handed radiation is sampled.

Additionally, we calculate the LDOP and circular degree of polarization (CDOP) using the following:

$$\text{LDOP} = \frac{\sqrt{S1^2 + S2^2}}{S0} \quad (11)$$

and

$$\text{CDOP} = S3/S0. \quad (12)$$

Finally, we should note that for all samples measured, $S2$, $S3$, and subsequently CDOP, were found to be within the noise of the experiment and were taken to be zero.

3. Results: Surface Roughness

To establish a baseline set of measurements, we considered a smooth substrate first. Figure 4 shows the spectral LDOP as a function of angle of incidence for the smooth glass sample held at a temperature of 65 °C. Also shown in the figure is a series of Fresnel calculations conducted for an arbitrary wavelength of 9.28 μm, where the complex indices n and k of figure 1 were used (see triangular data points). As one can see in figure 4, agreement between the measured LDOP and the Fresnel-calculated LDOP is quite good. Other Fresnel calculations conducted at other wavelengths showed similarly good agreement.

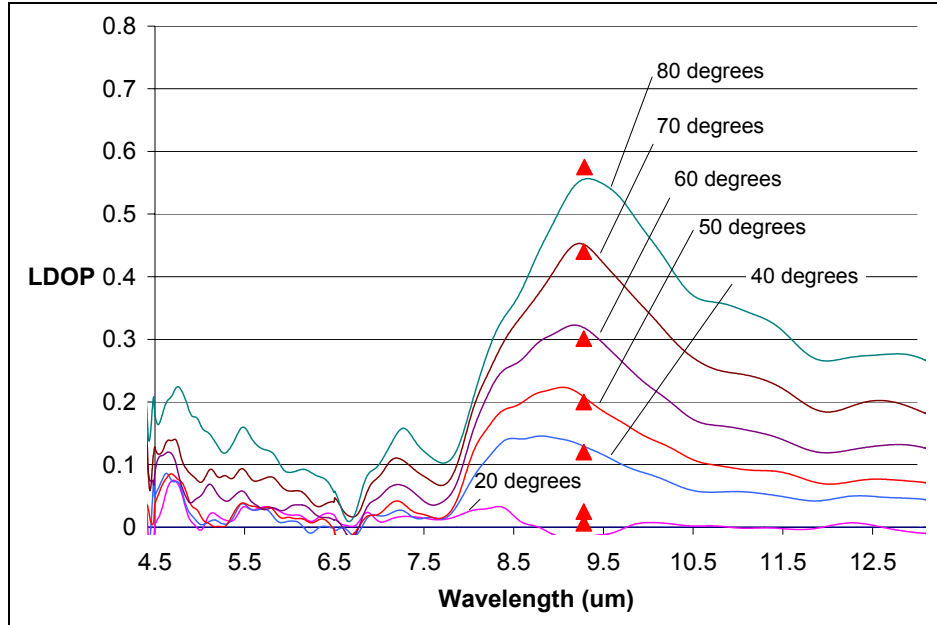


Figure 4. Measured LDOP as a function of wavelength and angle of incidence for a smooth borosilicate glass substrate heated to 65 °C. (Also shown [triangular data points] is the corresponding calculated LDOP for an emission wavelength of 9.28 μm based on the Fresnel relations of equations 4 through 6.)

Figures 5 through 7 show a similar series of measurements for the three roughened plates. As one can see in these figures, a noticeable reduction in the measured LDOP occurs as the glass substrates become progressively rougher.

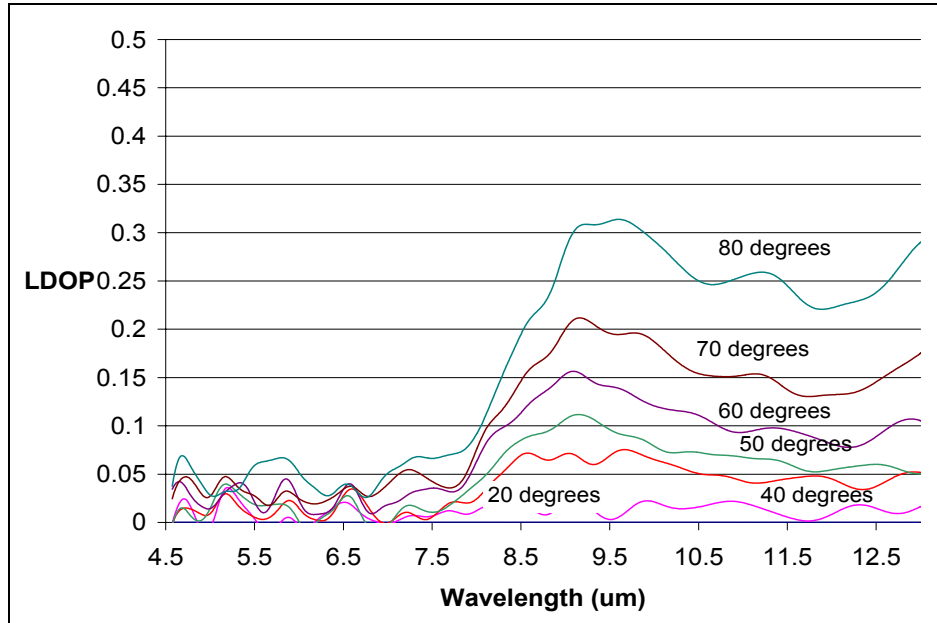


Figure 5. Measured LDOP for a lightly roughened borosilicate plate with $\text{Ra}=3.98\mu\text{m}$ and rms slope=9.67 degrees, as a function of wavelength and angle of incidence. (Plate temperature was held at 65 °C.)

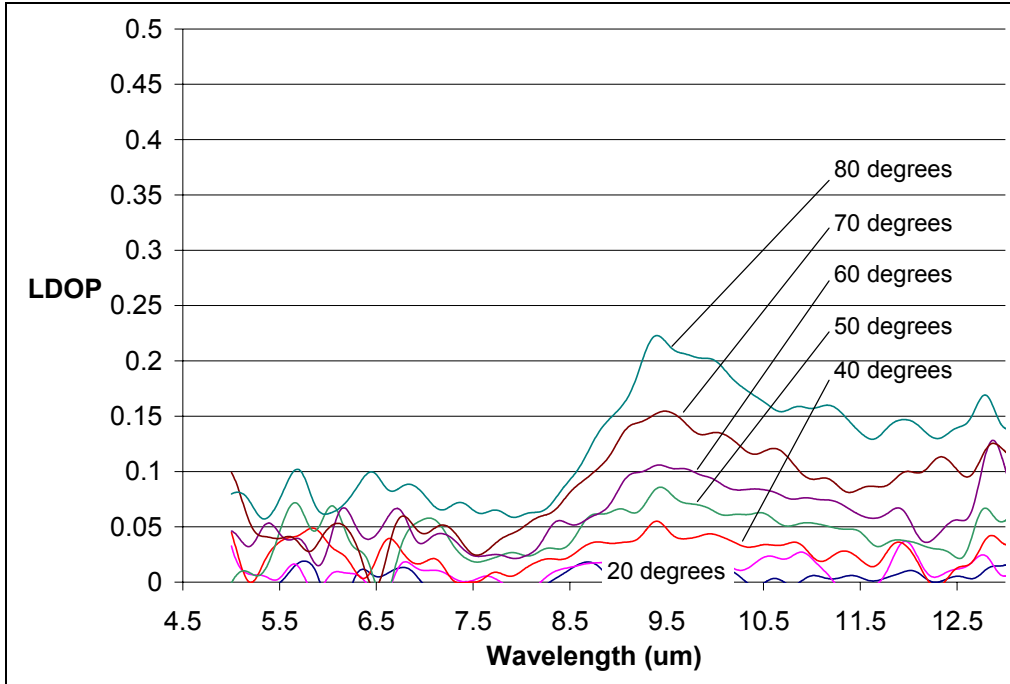


Figure 6. Measured LDOP for a moderately roughened borosilicate plate with $Ra=4.80\mu\text{m}$ and rms slope=8.60 degrees, as a function of wavelength and angle of incidence. (Plate temperature was held at 65 °C.)

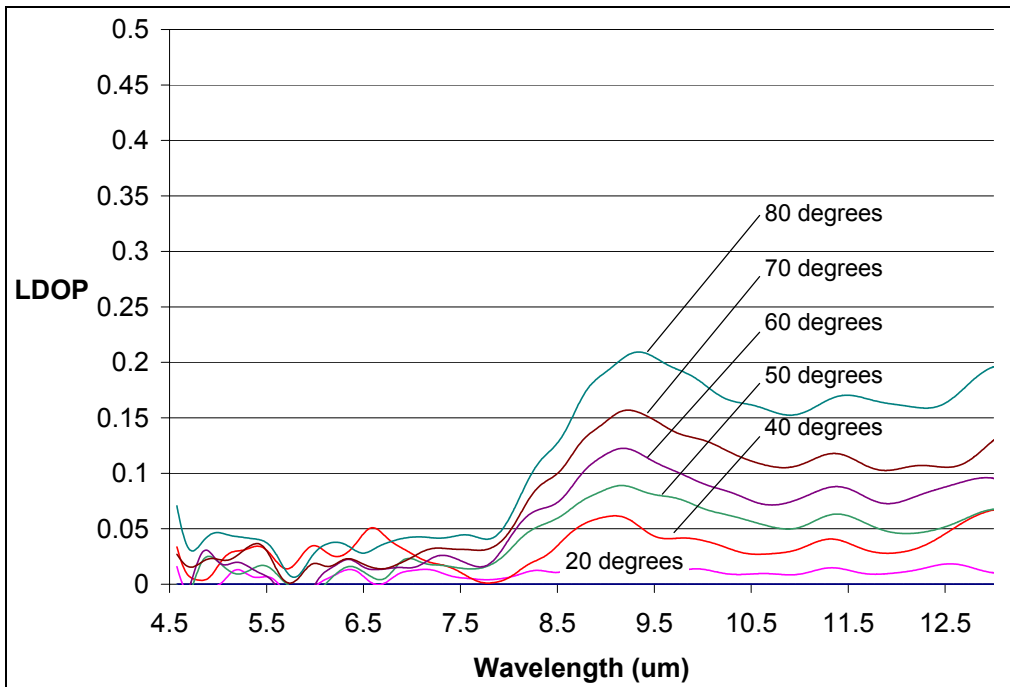


Figure 7. Measured LDOP for a very rough borosilicate plate with $Ra=6.68\mu\text{m}$ and rms slope=11.90 degrees, as a function of wavelength and angle of incidence. (Plate temperature was held at 65 °C.)

We contrast the strong spectral dependence of the LDOP shown in figures 4 through 7 by examining what happens to the same substrate when a thin dielectric layer is applied, i.e., a painted substrate. We considered two types of coatings of particular interest, 1) a common commercially available “Krylon¹” black spray paint and 2) a chemical agent-resistant coating (CARC) paint which is a multi-component epoxy resin often used on military vehicles.

Figures 8 and 9 show the measured LDOP for the two smooth painted surfaces. In applying the paints, we intentionally coated the surfaces with relatively thick layers in order to reproduce conditions most often seen in real-life applications. As a result, the spectral characteristics of the paint/substrate combination seen in figures 8 and 9 are primarily a function of the pigment only. As seen in both figures, the strong spectral characteristics seen for the plain glass plate are completely suppressed by somewhat featureless spectral emissivity for the two paints considered.

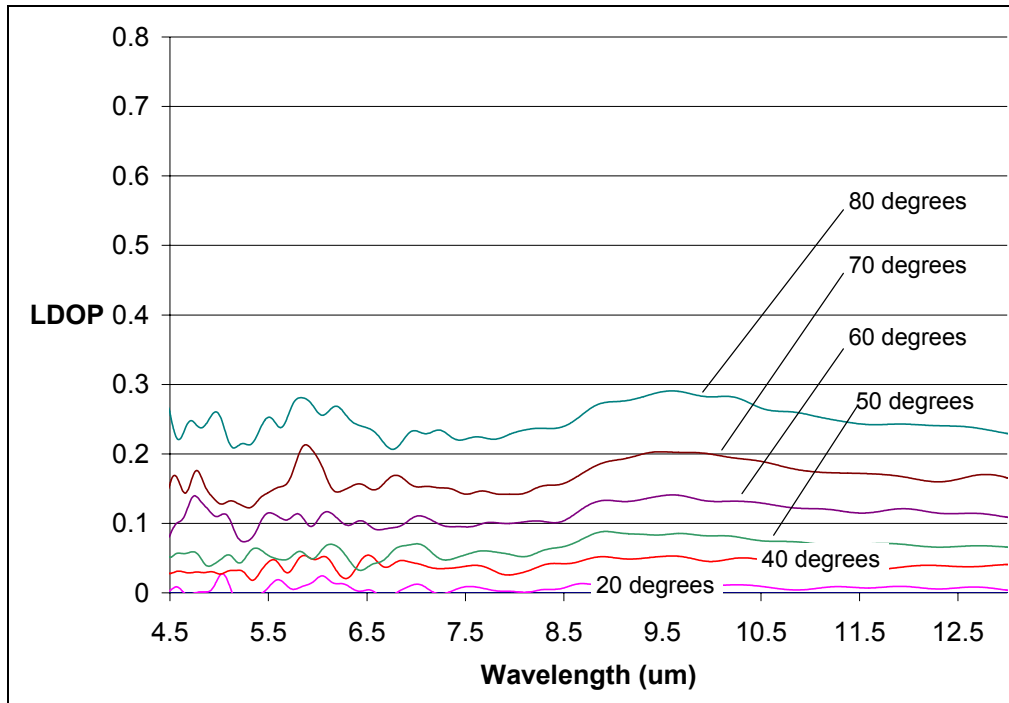


Figure 8. Measured LDOP as a function of wavelength and angle of incidence for a smooth borosilicate plate coated with a thin layer of black Krylon paint. (Plate temperature was held at 65 °C.)

¹Krylon® is a registered trademark of the Sherwin-Williams Company.

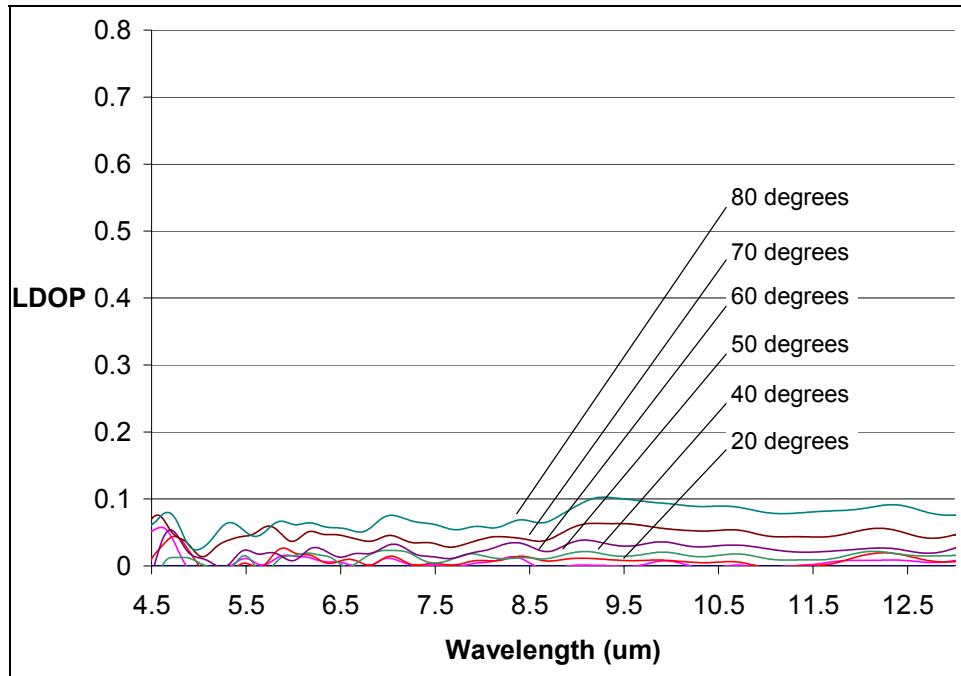


Figure 9. Measured LDOP as a function of wavelength and angle of incidence for a smooth borosilicate plate coated with a thin layer of a green CARC paint. (Plate temperature was held at 65 °C.)

4. Experiment: Dew Formation and Aerosol Contamination

The second portion of our study involved measuring the attenuation of polarized surface emission attributable to either dew formation or aerosol contamination. Again, smooth borosilicate glass substrates are mounted to a rotation plate that allows for continuous orientation of the surface normal from 0 to 90 degrees. In order to induce an initially strong LDOP, the test plates are positioned at a near horizontal angle of 80 degrees (see figure 10).

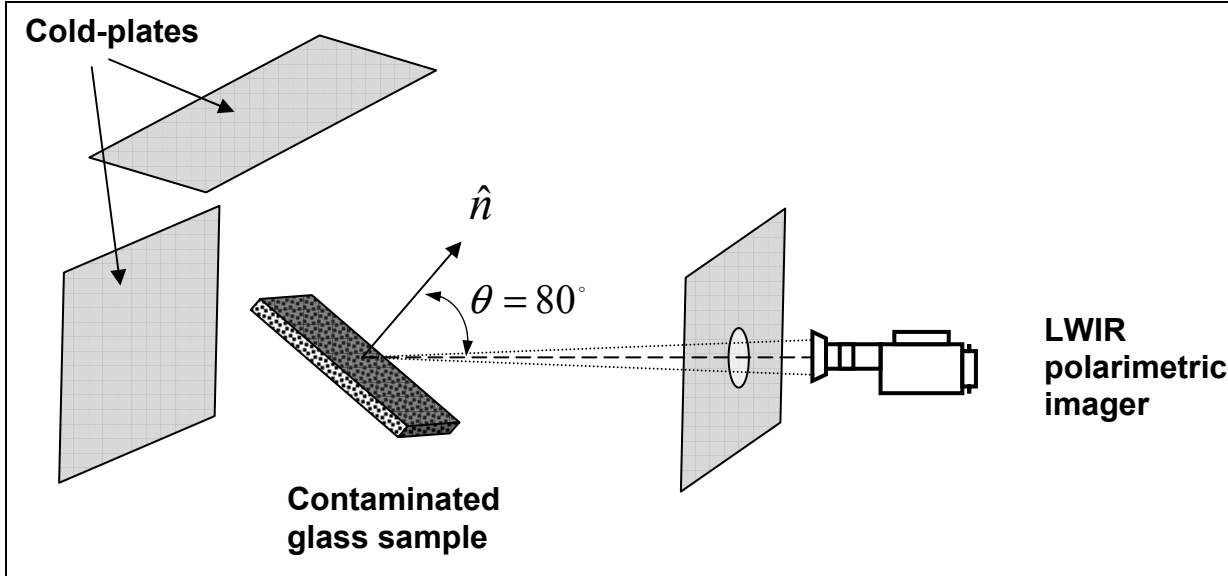


Figure 10. Diagram showing the experimental setup used for the dew/aerosol contamination study. (The test plate is oriented at a fixed angle of 80 degrees and held at room temperature.)

For this particular study, substrates are maintained at or near room temperature in order to facilitate dew formation. Samples for both the dew and particulate contamination study are placed in a large 2.0-m³ chamber that allows for controlled dissemination of either water vapor (dew) or one of the three aerosol particulates (i.e., carbon black, KBr powder, and orchard grass pollen).

When one is conducting IR measurements on objects at or below room temperature, great care must be taken to reduce or eliminate all ambient thermal radiation inherent to the laboratory. We eliminated much of the ambient laboratory-induced thermal radiation by placing a series of cold shields at various locations about the sample. Cold plates are held at a temperature of -10 °C by the circulation of a chilled ethylene glycol and water mixture through copper lines embedded in the cold plates.

To detect the room temperature emittance generated by the contaminated substrates, a new/novel polarimetric LWIR thermal imager is used. The imaging system consists of two primary components: a polarimetric module that houses a spinning achromatic cadmium selenide (CdSe) wave plate mounted in series with a fixed wire-grid polarizer, and a camera module that consists of a liquid nitrogen-cooled, 240x360 pixel, mercury cadmium telluride (HgCdTe) focal plane array (16). The spectral response for the FPA is limited to the waveband region 8.5 to 10.5 μm.

Before each run, the camera gain and offset are adjusted to take advantage of the FPA/frame grabbers' full dynamic range. Sequential LWIR polarimetric images of the test plates are recorded digitally at a rate as fast as 240 images/second and synchronized to the rotation of the spinning CdSe wave plate. The spinning wave plate and fixed wire-grid polarizer combination effectively acts like a variable polarimetric filter. As a result, each digital image recorded is

generated by polarized emittance of a particular state. Although the maximum acquisition rate is 240 frames/second, the present data were acquired at 128 frames/second. With the speed of the spinning wave plate set at 8 revolutions/second, 16 frames were measured every 125 ms and averaged over many revolutions. The averaged frames were then used in conjunction with the calibration files to determine all four Stokes parameters.

The obvious limitation of a “sequential frame” approach used here is that the test object must be stationary for an exposure period of at least 125-msec. Because our particular test objects were stationary, we could, if needed, operate at the full 240-Hz frame rate and average over many Stokes images to produce a better S/N ratio.

We calibrate the LWIR polarimetric imager by recording the radiometric response when we observe known linear and circular polarization states. We generate known states by polarizing the radiance from a high precision, 14- by 14-inch extended area blackbody. Radiance is linearly and circularly polarized by the identical wire-grid/quarter wave rhomb combination described in the spectro-polarimetric measurement. This allowed for exposure of the camera system to known linear and circular polarization states that are as close to ideal as possible (i.e., to provide uniform coverage over the entire Poincare sphere). A set of calibration frames is generated at the beginning and ending of each day. Each image frame represents one of the six necessary states needed to calculate the four Stokes vectors seen in equations 7 through 10, i.e., $I(0^\circ)$, $I(90^\circ)$, $I(\pm 45^\circ)$, $I(R)$, and $I(L)$. These calibration files are used to calculate the system’s modulation transfer function (MTF), which is used later to correct for any aberrations observed during the measurement and to calculate the Stokes parameters.

When one is considering contamination attributable to dew formation, warm humid air is generated by the evaporation of distilled water via a commercially available humidifier and is directed into the test chamber via a 4-inch-diameter vent. The water vapor quickly begins condensing on the cooler glass surface, and small micron-size dew particles begin to form (see figure 11).

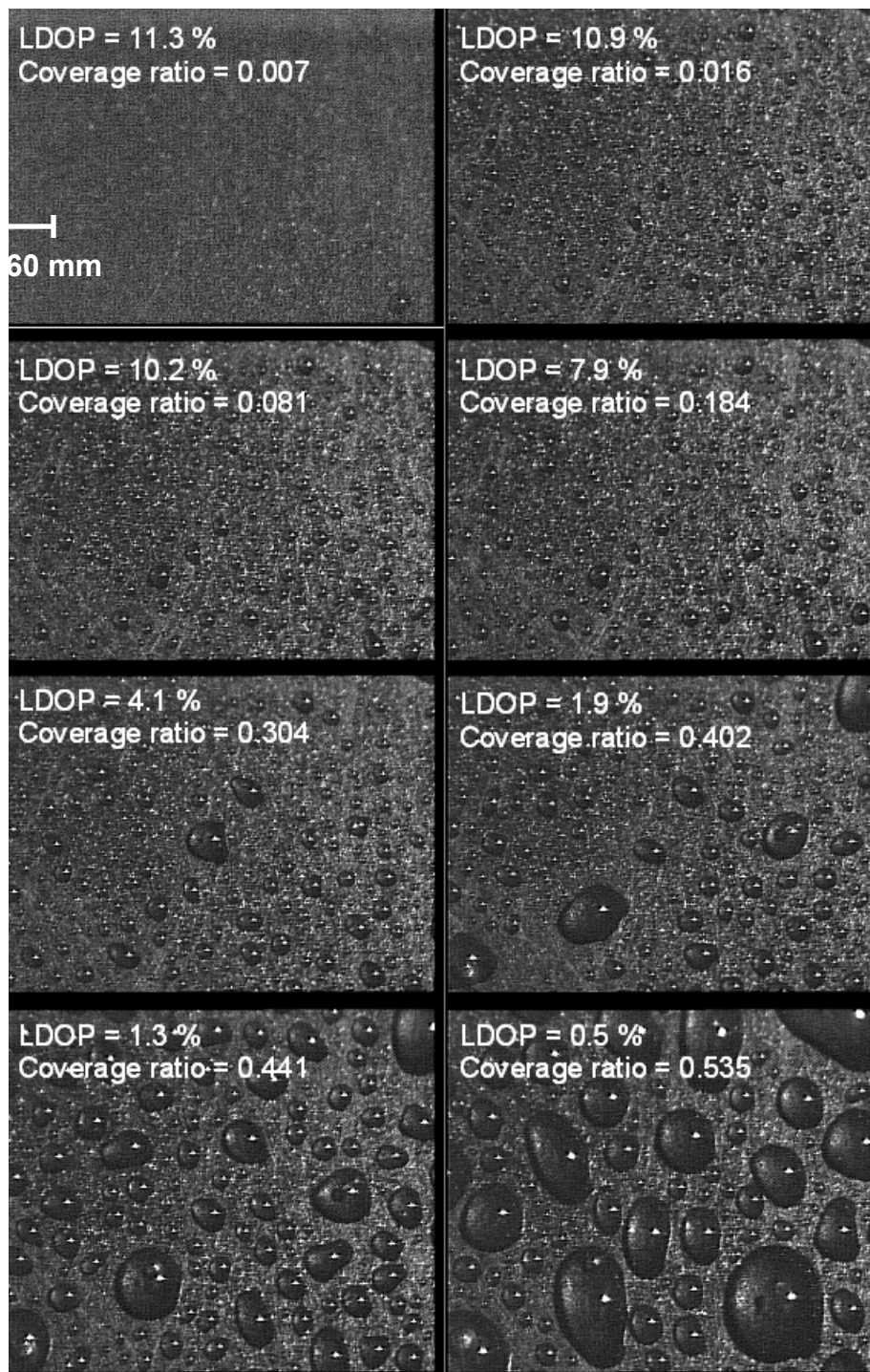


Figure 11. Video image series showing the dew condensation process. (Shown in each image is the corresponding coverage ratio, [i.e., surface area covered divided by the total area], and the corresponding measured LDOP for $\theta=80^\circ$.)

Polarimetric data are recorded continuously as the dew-forming process continues. Data are recorded until either the dew droplets grow to form a continuous layer or the LDOP is no longer measurable. A sample thermal polarimetric image used to determine the emitted LDOP is seen in figure 12. The chamber is evacuated, the target plate cleaned, and the polarimetric measurement is repeated.

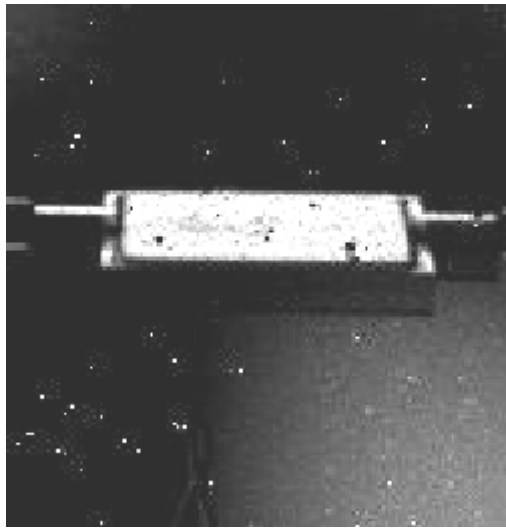


Figure 12. Sample calibrated LWIR polarimetric image used to determine the LDOP for a smooth glass substrate contaminated by a modest amount of carbon black particles. (LDOP is determined from the gray scale values for the pixels that represent the heated glass surface.)

Three types of aerosols are considered for the contamination portion of the study. Each particulate chosen was based on the degree of optical absorption that each material possessed, i.e., finely milled KBr particles (weak absorber), orchard grass pollen particles (moderate absorber), and carbon black (strong absorber).

To generate varying degrees of particulate contamination, the test substrate is placed in a 2.0-m³ chamber. In order to aerosolize the particulates efficiently, a specially designed pneumatic nozzle was constructed. Dry pressurized air is used to inject the particulates through a cylindrical nozzle that contains a spiraling array of fine stainless steel wires. A vortex created within the nozzle effectively separates and disperses the particles with minimal agglomeration.

A small quantity of the particulate (typically less than 0.20 gram) is placed in the dispersing nozzle and is injected into the sealed chamber. A small fan in a corner of the chamber is used to stir the aerosol to ensure that a uniform distribution is achieved. The fan is turned off and the aerosol is allowed to settle onto the target plate.

A real-time video log of the contaminating process is recorded periodically during the polarimetric measurement. We accomplished this by swinging a high-power video microscope into a fixed position slightly above the test surface. Once a series of images is recorded, the video microscope is removed and the recording of the LWIR polarimetric data continues. Later, analysis of the digital images is used to determine particle size, shape, and concentration; for example, see figures 11 and 13. Although not easily seen from the images of figure 13, qualitative, analysis conducted on the samples yielded an approximate nominal diameter range of 0.20 to 0.35 μm for carbon black, 0.5 to 0.8 μm for KBr, and 30 to 40 μm for the orchard pollen (17).

The polarimetric measurement is conducted on each plate with the same procedure described in the dew portion. Once a set of measurements is completed, the plate is removed, subjected to further contamination, and remeasured.

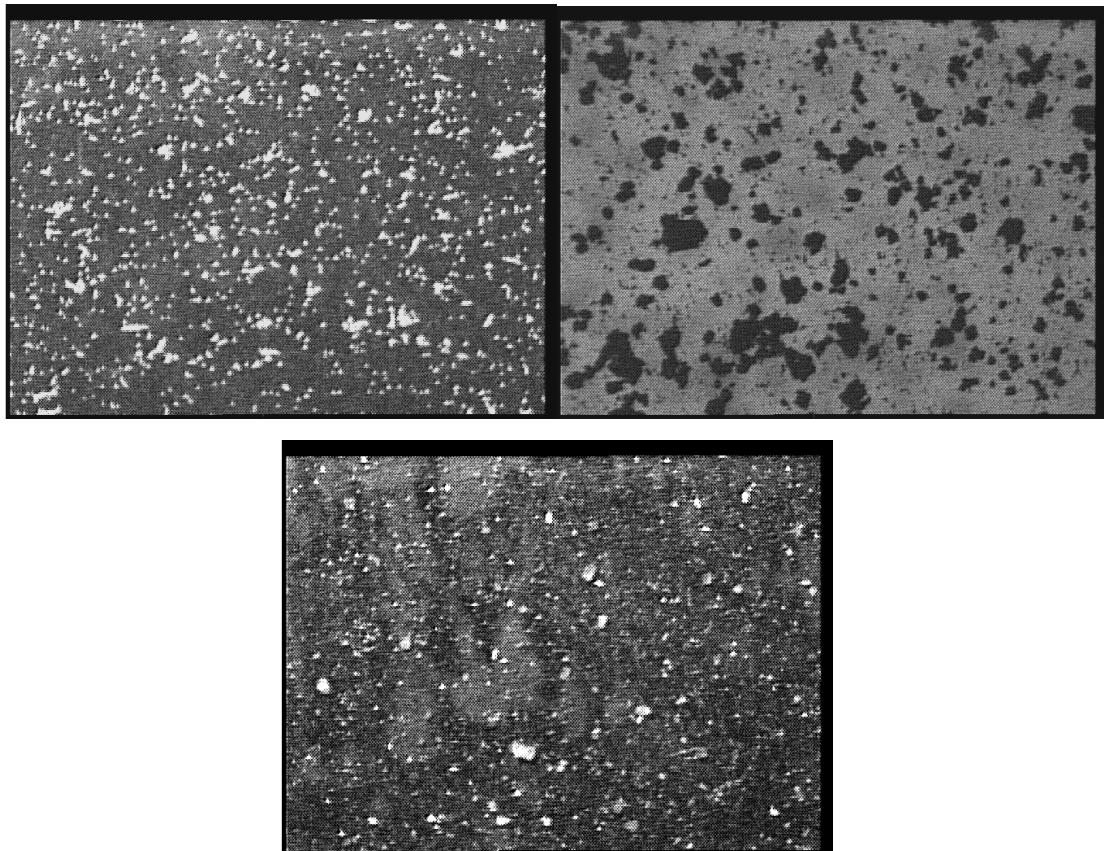


Figure 13. Sample visible images showing various forms of aerosols contamination considered, i.e., orchard pollen (top left), carbon black (top right), and KBr particles (bottom).

5. Results: Dew Formation and Aerosol Contamination

Figure 14 shows the measured and calculated LDOP for varying degrees of dew coverage. Each data point shown represents a single polarimetric measurement in which we calculated the coverage ratio (i.e., covered surface area divided by the total surface area) by analyzing a series of photographs similar to those seen in figures 11 and 13. Also shown in figure 14 is the corresponding geometric-based calculation in which the complex index for water and the glass substrate is taken to be $1.193+0.05i$ and $2.4+0.5i$, respectively, for the waveband region 8.5 to $10.5\text{ }\mu\text{m}$ (12,18,19). Figure 15 shows a similar set of measurements except now the contaminating medium consists of a variety aerosol particulates, i.e., carbon black, KBr powder, and pollen.

Finally, because each data point seen in figures 14 and 15 represents a single measurement, rather than a statistical average of values, uncertainties inherent to the measurement are best represented by examination of the magnitude of scatter within the data. Since we determine the coverage ratios by applying a machine vision algorithm to a series of photographs, the error associated with these values is primarily related to the number of sample images used. We found little variation in coverage ratio after analysis of approximately 10 to 12 images. For most data seen in figures 14 and 15, the number of images used in the analysis often exceeded 20 frames. As a result, we believe the uncertainty associated with determining the coverage ratio to be less than 5 to 7%. Analysis of the polarimetric calibration yield uncertainties on the order of 10 to 18% primarily because of limitations of the wire-grid polarizer, i.e., the extinction ratio for the wire grid was found to be approximately 170 over the wavelength range of 8.5 to $10.5\text{ }\mu\text{m}$.

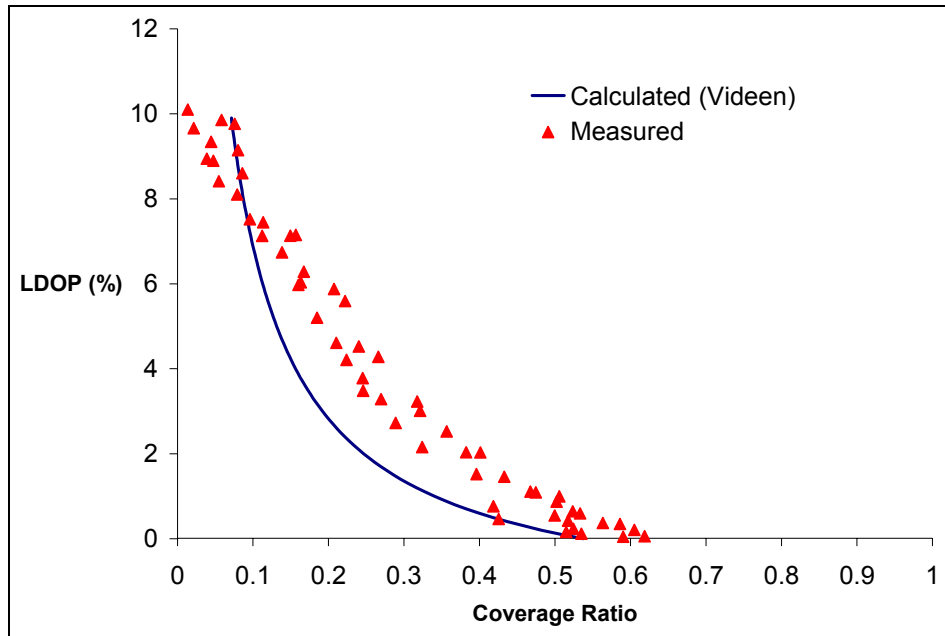


Figure 14. Measured LDOP for varying degrees of dew (water) coverage on the surface of a smooth borosilicate glass substrate at 22 °C, $\theta=80^\circ$. (Also shown is the calculated LDOP by the geometric approach of Videen (12).)

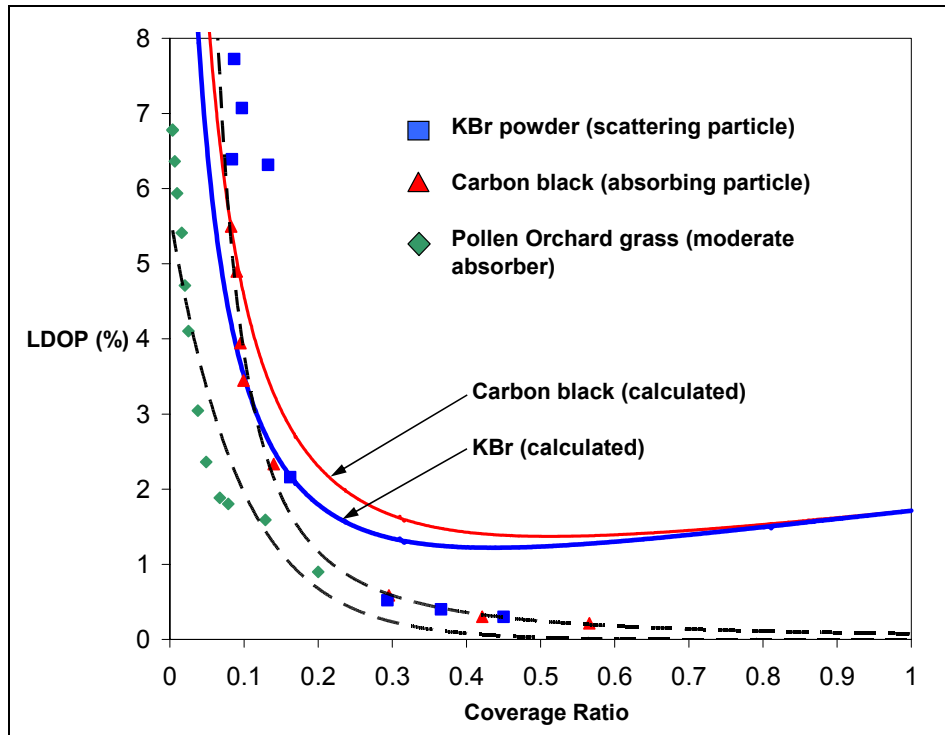


Figure 15. Measured LDOP for a smooth borosilicate glass plate held at 22 °C, contaminated with varying degrees of carbon black, KBr particles, or pollen, that were evenly dispersed on the surface. (Substrates mounted at $\theta=80^\circ$ [the dashed line shown represents the corresponding curve fit]. Also shown is the calculated LDOP based on the geometric approach put forth by Videen.)

6. Discussion

When we entered into the surface roughness study, we had hoped to create a sample set of roughened surfaces that spanned as large a range as possible. Inspection shortly after bead blasting of the glass surfaces suggested that a broad range of roughness values had been achieved. It was only much later during the formal surface characterization process that we realized the limited range values for either Ra or the localized rms slope, i.e., our values ranged from Ra = 3.98 to 6.68 μm and rms slope 8.60 to 11.90 degrees. We attribute our inability to generate a more diverse set of test surfaces to the crystalline structure of the borosilicate glass plates. Jordan and Lewis experienced similar limitations in creating test surfaces of either glass or aluminum. Initially, we had hoped to create a surface so diffuse that the measured emittance showed no preferential polarization. Neither we nor Jordan were able to produce such conditions. For angles of orientation in excess of 40°, we report a measurable LDOP for all roughened samples considered.

Although the rms slope distribution is thought by many theorists to be the most important parameter influencing the attenuation of polarized emission attributable to surface roughness, in practice, accurate determination of this parameter is quite problematic. Bennett et al. reports that even during the best of conditions, measurement of the rms slope can vary by as much as a factor of 50 from one practitioner to another, depending on the instrumentation used, cutoff length, profilometer stylus geometry, scan rate, etc. (20). Much of the emphasis placed on the use of the rms slope is based on the premise that roughened surface facets may be treated as series of infinitesimally small planar surfaces oriented at various angles described by the rms slope distribution. Even if good reproducible rms slope values exist, researchers must then “assume” a type of distribution to apply the rms measurement to that distribution. For example, Jordan and Lewis report significant variance in the calculated LDOP for a series of roughened surfaces, depending on whether a Gaussian or Cauchy distribution is applied (7). Regardless of the difficulty inherent to measuring an accurate surface profile, it is not entirely clear that a simple geometric approach is truly valid when the dimensions of the facets are comparable or smaller than the emission wavelength, as is the case here.

Finally, figure 16 shows a comparison of measured LDOP values taken at the emission wavelength 9.90 μm as a function of surface roughness and orientation. Also shown are the LDOP results of Jordan and Lewis for their roughened glass substrate, Ra = 9.89 μm and rms slope = 24.5 degrees (7). One startling feature seen in figure 16 is that with the exception of a few data points for the Ra = 3.98 μm sample, the measured functional dependence appears to be the same for all roughened samples considered (including those of Jordan and Lewis), regardless of surface roughness parameter or rms slope. One would hope to see different polarimetric responses as the substrates transition from a specular to a diffuse surface as the roughened facets

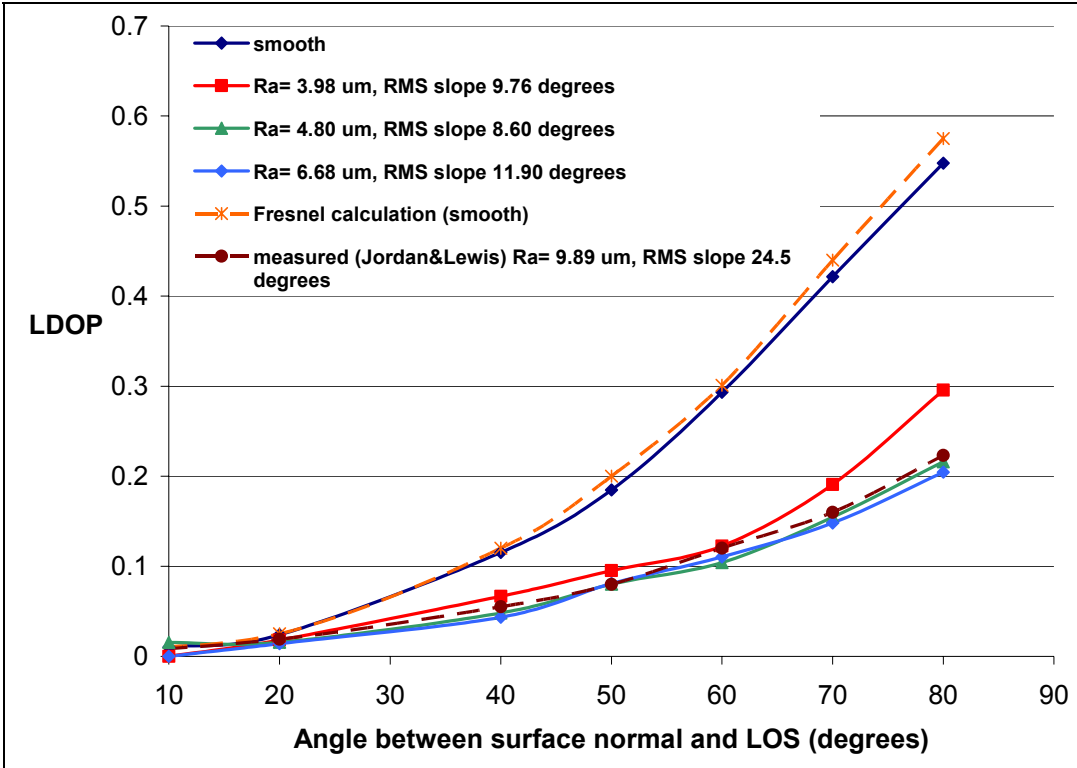


Figure 16. Comparison of measured LDOP (taken at $9.90 \mu\text{m}$) as a function substrate orientation for various roughened glass plates. (Also shown are the measured and Fresnel-based calculations for smooth glass substrates [top dashed line] and results from Jordan and Lewis [bottom dashed line] (7).)

become larger. We speculate that this apparent insensitivity to changes in various surface features is attributable to an insufficient range of Ra values considered. We believe the transition from specular to diffuse surfaces in the measured LDOP would be evident if more moderately roughened samples were examined, e.g., Ra values between 0.5 and 2.0 μm . An informal survey of measured Ra values (measured with a hand-held profilometer) taken from numerous civilian and military type vehicles shows a fairly narrow range of Ra values, i.e., 0.02 to 3.65 μm , where the higher values could be loosely described as quite abrasive.

The spectrally resolved LDOP shown in figures 4 through 7 highlights the strong wavelength dependence that polarized thermal emission exhibits for certain types of materials. As a result, care must be taken to ensure that all spectral dependences for the surface being considered (as well as the polarimetric optics used for the measurement) are well defined. For example, consider figure 4. It is apparent that one would get quite different values for the measured LDOP if the responsivity of the instrument is limited (either by optical components or the detector) to a narrow band about 9.4 μm or is allowed to integrate over a wider wavelength region, say 8.0 to 9.5 μm .

We had hoped to highlight this point further by applying various coatings to the surface (i.e., black Krylon and CARC paint), but unfortunately, the pigments chosen did not exhibit the complex emission spectra we had originally hoped for. Rather, one can see from figures 8 and 9 that the paints chosen exhibited emission spectra that are fairly featureless, compared to figure 4, and suppressed the underlying emission from the heated borosilicate glass substrate.

Now let us consider the dew/aerosol contamination portion of the study. As mentioned earlier, the LDOP is a measure of asymmetry exhibited by a sample. An asymmetric system/particle tends to emit a preferred polarization signal, whereas, a symmetric system/particle has no preferred polarization emission and its radiometric contribution results in unpolarized noise. In our samples, the smooth plane substrate provides a polarized signal, whereas, the randomly oriented particulates provide the noise. These particles not only reduce the polarization by contributing an unpolarized component to the total signal, but also shadow the substrate, preventing the polarized signal from reaching the detector. As one can see from figures 14 and 15, the total attenuation of the LDOP occurs for all contaminants considered as the coverage ratio approaches 0.5 to 0.6 (note that coverage ratios are determined for observation along the surface normal). Since all dew/aerosol contaminant measurements are conducted while the plates are orientated at a high grazing angle of 80° degrees, the projected shadows cast by the particles on the plane surface at this angle are nearly 6 times their size at normal incidence. The particles cast their shadows not only on the substrate but also on other particles. The shadowing of particles by other particles is not random and tends to cover the bottom portion of the particles, disrupting their symmetry. As a result, this asymmetric shadowing may be considered another source of the polarization signal (12). With no particle-on-particle shadowing, the LDOP response shows a linear decrease proportional to the coverage ratio. Partial shadowing of particles introduces a new nonlinear term. For relatively small coverage ratios, we expect partial shadowing to be negligible and the LDOP to show a linear decrease. This linear term approaches zero for spherical contaminants when the coverage ratio equals the cosine of the detection angle. If the particles are oriented with 100% efficiency so that they cast their shadows only on the plane surface and not on other particles, the LDOP would equal zero at coverage ratios of approximately 17%. As the coverage ratio increases, we expect to see a nonlinear term to be introduced that gives rise to a tail in the LDOP signals shown in figures 14 and 15.

It is significant that figure 14 shows a nearly linear response of the LDOP to coverage ratio. We attribute the divergence between measured and calculated LDOP at intermediate values of the coverage ratio to the fact that the calculations assume a monodispersed drop size for dew. The nonlinear response seen in the model calculations results from shadowing of dew particles by other dew. In this case, the bottom portions of the dew are shadowed and a nonlinear term is introduced into the total LDOP signal. However, the dew shown in figure 11 is far from monodispersed. The dew consists of some large particles and many smaller particles. As a result, the shadowing is non-uniform. Either a small portion of the bottom of the large particles is shadowed by smaller particles, or entire small particles are shadowed by large particles.

Partial shadowing plays a minor role. As a result, the nonlinear term in the LDOP is suppressed, and the resulting measured response is nearly linear, as is seen in figure 14.

Figure 15 shows the LDOP response measured from three other atmospheric aerosol particles: pollen, carbon black, and KBr particles. When one is comparing figures 11 and 13, it is apparent that these particles have a narrower size distribution than the dew particles. The percentage of large or agglomerated particles is much lower than that for the dew sample, so there is a significant amount of partial shadowing of other particles, rather than complete shadowing, as seen in the dew sample. As a result, the LDOP for these particles shows a much stronger nonlinear term than that of the dew particles, demonstrating that partial shadowing plays a significant role in determining the LDOP for these systems.

We note that the LDOP for the highly absorbing carbon black is nearly identical to the transparent KBr particles. This should not be cause for concern. The particles composing the samples are non-spherical, and the LDOP is the average signal over this shape polydispersity. Just as two completely different scattering systems may have similar scattering coefficients, they also may have similar LDOPs. However, the carbon and KBr particle systems have a common feature that may also explain this similarity: they are both agglomerates of Rayleigh-size particles. The nominal sizes of the individual components comprising these particle systems are submicron. Like polarized Rayleigh scattering, polarized emission from particles small compared to the wavelength does not depend on particle emissivity. This appears to be reflected in the properties of the agglomerated particle systems shown in figure 15. It is interesting to note that as the surface density of these agglomerated particles increases, the LDOP response is very similar to the theoretical response shown in figure 14. Although the theoretical description of Videen is wholly inadequate to describe this system, it appears from the nonlinear shape of these curves that partial shadowing is a primary physical mechanism.

Figure 15 also shows the LDOP of the orchard pollen particles. These particles are not Rayleigh, being 30 to 40 μm in size; however, their shape is irregular and composition is heterogeneous. It is apparent in this case that the nonlinear shadowing term is a significant component for this system. The LDOP response of the orchard pollen is reduced significantly from that of the two Rayleigh agglomerates.

Finally, we should note that because the carbon and KBr particles are sub-micron, we were unable to resolve visible images until the particulates agglomerated into larger sizes, say 1.0 μm , and that is the reason there are no coverage values below 0.10.

7. References

1. Sandus, O. A review of emission polarization. *Appl. Opt.* **1965**, *4* (12), 1634–1642.
2. Bertilone, D. C. Stokes parameters and partial polarization of far-field radiation emitted by hot bodies. *J. Opt. Soc. Am. A* **1994**, *11* (8), 2298–2304.
3. For an excellent treatment of the directional properties associated with thermal radiation see; Siegel, Robert; Howell, J. R. *Thermal Radiation Heat Transfer*; McGraw-Hill Co.: New York, 1981.
4. Tooley, R. Man-made target detection using Infrared polarization. *SPIE Conf. Polarization Considerations for Optical Systems II* **1989**, *1166*, 52–58.
5. Cooper, A.; Lentz, J. Infrared polarization ship images and contrast in the MAPTIP Experiment. *SPIE* **1996**, *2828*, 85–96.
6. Rogne, T.; Smith, F. Passive target detection using polarized components of infrared signatures. *SPIE Polarimetry: Radar, Infrared, Visible, Ultraviolet, and X-Ray* **1990**, *1317*, 242–251.
7. Jordan, D. L.; Lewis, G. D. Emission polarization of roughened glass and aluminum surfaces. *Appl. Opt.*, *35* (19), 3583–3590.
8. Jordan, D. L.; Lewis, G. Measurement of the effect of surface roughness on the polarization state of thermally emitted radiation. *Opt. Letters* **1994**, *19* (10), 692–694.
9. Shaw, J. A. Degree of linear polarization in spectral radiances from water-viewing infrared radiometers. *Appl. Opt.* **1999**, *38* (15), 3157–3165.
10. Shaw, J. A.; Marston, C. Polarized infrared emissivity for a rough water surface. *Optics Express* **2000**, *7* (11), 375–380.
11. Chang, P. C.; Flitton, J. C. Importance of shadowing and multiple reflections in emission polarization. *Waves in Random Media* **2002**, *12* (1), 1–19.
12. Videen, G. Polarized Infrared Emissivity from Dew Droplets on a Surface. *Appl. Opt. LP* **2003**, *42* (27), 5557–5560.
13. Chenault, D.; Chipman, R. Infrared spectropolarimetry. *SPIE Symposium on Polarization Considerations for Optical Systems II* **1989**, *1166*, 254–266.
14. Lane, D. W. The optical properties and laser irradiation of some common glasses. *J. Phys. D: Appl. Phys.* **1990**, *23*, 1727–1734.

15. Crandall, D. G.; Chipman, R. A. Polarization aberration of crossed folding mirrors. *Novel Optical Systems Design and Optimization, Proc. SPIE* **1995** 2537, 83–93.
16. Chenualt, D.; Chipman, R. Infrared birefringence spectra for cadmium sulfide and cadmium selenide. *Appl. Opt.* **1993** 32 (22), 4223–4227.
17. Putscher, R.; McCrone, W. C. *Characterization of air particles giving false responses with biological detectors*; Tech. # ED-CR-75025, Edgewood Arsenal Technical Report: National Technical Information Service, July 1975.
18. Segelstein, D. J. Complex refractive index of water. MS Thesis, University of Missouri, Kansas City, MI, 1981.
19. Lane, D. W. The optical properties and laser irradiation of some common glasses. *J. Phys. D: Appl. Phys.* **1990**, 23, 1727–1734.
20. Bennet, J. M.; Mattson, L. *Introduction to Surface Roughness and Scattering*; Optical Society of America Press: Washington D.C. (1989).

Distribution

ADMNSTR	US MILITARY ACDMY
DEFNS TECHL INFO CTR	MATHEMATICAL SCI CTR OF EXCELLENCE
ATTN DTIC-OCP (ELECTRONIC COPY)	ATTN LTC T RUGENSTEIN
8725 JOHN J KINGMAN RD STE 0944	THAYER HALL RM 226C
FT BELVOIR VA 22060-6218	WEST POINT NY 10996-1786
DARPA	SMC/GPA
ATTN IXO S WELBY	2420 VELA WAY STE 1866
3701 N FAIRFAX DR	EL SEGUNDO CA 90245-4659
ARLINGTON VA 22203-1714	
OFC OF THE SECY OF DEFNS	US ARMY ARDEC
ATTN ODDRE (R&AT)	ATTN AMSTA-AR-TD
THE PENTAGON	BLDG 1
WASHINGTON DC 20301-3080	PICATINNY ARSENAL NJ 07806-5000
US ARMY TRADOC	US ARMY AVIATION & MIS LAB
BATTLE LAB INTEGRATION & TECHL	ATTN AMSAM-RD-MG-IP
DIRCTRTR	H F ANDERSON (20 COPIES)
ATTN ATCD-B	REDSTONE ARSENAL AL 35809
10 WHISTLER LANE	
FT MONROE VA 23651-5850	US ARMY AVN & MIS CMND
 	ATTN AMSMI-RD W C MCCORKLE
DIR FOR MANPRINT OFC OF THE	REDSTONE ARSENAL AL 35898-5240
DEPUTY CHIEF OF STAFF FOR PRSNNL	
ATTN J HILLER	US ARMY CECOM RDEC NVESD
THE PENTAGON RM 2C733	ATTN J HOWE
WASHINGTON DC 20301-0300	10221 BURBECH RD STE 430
 	FT BELVOIR VA 22060-5806
EDGEWOOD CHEMICAL BIOLOGICAL CTR	US ARMY ECBC
ATTN AMSSB-RRT-DP A C SAMUELS	ATTN AMSSB-RRT BOTTIGER
ATTN AMSSB-RRT-DP	ATTN AMSSB-RRT E STUEBING
R VANDERBEEK	5183 BLACKHAWK RD BLDG E-5951
5183 BLACKHAWK RD BLDG E-5554	ABERDEEN PROVING GROUND MD 21010-5424
ABERDEEN PROVING GROUND MD 21010-5424	
	US ARMY INFO SYS ENGRG CMND
	ATTN AMSEL-IE-TD F JENIA
	FT HUACHUCA AZ 85613-5300

US ARMY NATICK RDEC
ACTING TECHL DIR
ATTN SBCN-TP P BRANDLER
KANSAS STREET BLDG78
NATICK MA 01760-5056

US ARMY SIMULATION TRAIN &
INSTRMNTN CMND
ATTN AMSTI-CG M MACEDONIA
12350 RESEARCH PARKWAY
ORLANDO FL 32826-3726

USAF ARMSTRONG LAB EDGEWOOD RDEC
ATTN AMSSB-RRT B BRONK
BLDG E-5951
ABERDEEN PROVING GROUND MD 21010

NAV RSRCH LAB
ATTN JD EVERSOLE
4555 OVERLOOK AVE
WASHINGTON DC 20375

HICKS & ASSOC INC
ATTN G SINGLEY III
1710 GOODRICH DR STE 1300
MCLEAN VA 22102

DIRECTOR
US ARMY RSRCH LAB
ATTN AMSRD-ARL-RO-D JCI CHANG
ATTN AMSRD-ARL-RO-EN W D BACH
PO BOX 12211
RESEARCH TRIANGLE PARK NC 27709

US ARMY RSRCH LAB
ATTN AMSRD-ARL-D J M MILLER
ATTN AMSRD-ARL-CI-EE G VIDEEN
ATTN AMSRD-ARL-CI-EE K GURTON
(10 COPIES)
ATTN AMSRD-ARL-CI-EE R DAHMANI
ATTN AMSRD-ARL-CI-IS MAIL & RECORDS
MGMT
ATTN AMSRD-ARL-CI-OK-T TECHL PUB
(2 COPIES)
ATTN AMSRD-ARL-CI-OK-TL TECHL LIB
(2 COPIES)
ATTN AMSRD-ARL-SE-EE A GOLDBERG
ATTN AMSRD-ARL-SE-EM D BEEKMAN
ADELPHI MD 20783-1197